(Received 4 December 2025, Accepted 25 December 2025, Scheduled 7 February 2026)

Compact Shared-Radiator Four-Element MIMO Antenna Module for 5G Terminals

Shuai-Peng Zhang[1] and Xiao-Mei Ni[2, *]

[1] School of Mechanical Engineering, Nantong University, Nantong 226019, China
[2] School of Aeronautic Engineering, Nanjing University of Industry Technology, Nanjing 210023, China

ABSTRACT: This work introduces a compact, low-profile, wideband multiple-input multiple-output (MIMO) antenna module designed for integration into 5G-enabled mobile terminals. The MIMO system comprises four patches with I-slots, each connected to one feed port. For a single patch, the slot controls and merges TM_{10} mode with TM_{01} mode, enabling dual-mode operation. Subsequently, shared-radiator technique is used, utilizing the coupling between the patches. When one patch is activated, it causes adjacent patches to become excited as well, resulting in a multi-patch operational mode that improves impedance matching. To ensure isolation, metallized vias are used to control coupling between elements, achieving an isolation level over 15 dB. The design measures a compact size of 28 mm × 28 mm × 1.5 mm. The prototype exhibits an impedance bandwidth of 4.34–5.06 GHz, confirming its practical usability in N79 band. It achieves over 40% efficiency and low envelope correlation coefficients (ECC). The design's compact size, good isolation, and ease of integration render it a suitable candidate for mobile terminals.

1. INTRODUCTION

The commercialization of fifth-generation (5G) networks highlights the pressing need for broader spectrum allocation and increased data processing capabilities in mobile devices. Enhancing the channel capacity of wireless systems has become a critical objective, and it can be effectively achieved by deploying a large number of antennas [1]. Thus, multiple-input multiple-output (MIMO) technology has garnered significant attention, as it leverages spatial multiplexing to boost system capacity without requiring additional bandwidth or transmit power [2, 3].

In mobile terminals, MIMO antennas can be installed on the frame or the chassis ground. Numerous MIMO designs for frame installation are currently available, as demonstrated by studies [4–9]. However, with the significant increase in antenna count, the available space on the frame is becoming increasingly limited. Consequently, the chassis ground offers a promising location for MIMO deployment, an area that has recently attracted growing research interest. Several designs installed on the chassis ground have been proposed. In [10], an eight-element MIMO antenna is introduced, utilizing multiple resonant modes to cover N79 band. In [11, 12], MIMO designs employ the multimode feature to cover multiple frequency bands. In [13], a MIMO design featuring a rotated L-shaped feeding probe is introduced, effectively exciting seven modes across a wide bandwidth of 5.14–9.05 GHz. However, achieving adequate isolation typically requires large element spacing, resulting in low space utilization. To address this, compact MIMO designs have been introduced to enhance spatial efficiency. In [14], four planar inverted F-shape antennas (PIFAs) are arranged in a sequentially rotated configuration, achieving a compact size and covering the 3.3–4.2 GHz band, with isolation exceeding 9.7 dB. In [15], a coupled-feed trapezoidal PIFA, a short-circuit trapezoidal monopole, and an L-shaped monopole branch enable the four-antenna system to cover the 3.3–5.0 GHz range, with isolation over 10 dB. In [16], triple modes (monopole mode, TM_{10}, and TM_{01}) are excited simultaneously to achieve wideband radiation, and the cross-line fence provides over 12 dB isolation across 2.394–2.530 GHz. However, due to smaller element spacing, the isolation between elements is relatively low, and there is still potential for further size reduction.

Shared-radiator MIMO configurations enhance space utilization more efficiently. In [17], two elements share the same structure, and two sets of degenerate characteristic modes along with a capacitive coupling feeding structure are utilized to achieve the bandwidth of 3.3–3.8 GHz and isolation of more than 20 dB. In [18], two elements share the same patch, and a bending slot is introduced to increase isolation between ports based on the principle of electrical and magnetic coupling cancellation. In [19], the central patch shares its space with the surrounding four elements to create an additional resonant point, and metallized vias are placed on the center patch to achieve the isolation over 12.5 dB. Although these designs have achieved effective space savings, they still have limitations, such as being restricted to only two elements [17, 18], having lower isolation levels and a higher profile [19] for mobile terminals.

This paper presents a low-profile, wideband four-element MIMO antenna designed for integration into the chassis of mobile terminals. The design features four square patches, each associated with a feed port. When a port is excited, its corresponding patch begins to function, and the surround-

* Corresponding author: Xiao-Mei Ni (18018035351@163.com).

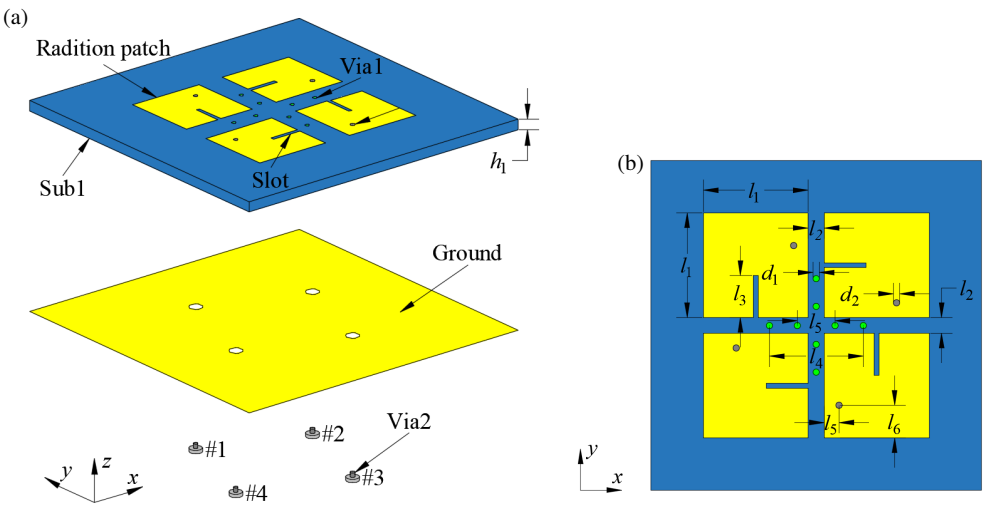

FIGURE 1. Structure of the proposed antenna. (a) Structure of the antenna. (b) Top view of the antenna. (Design parameters: $l_1 = 13.5$, $l_2 = 1.4$, $l_3 = 4.5$, $l_4 = 16$, $l_5 = 6$, $l_6 = 4.25$, $d_1 = 0.2$, $d_2 = 0.4$, $h_1 = 1.5$. Units: mm.)

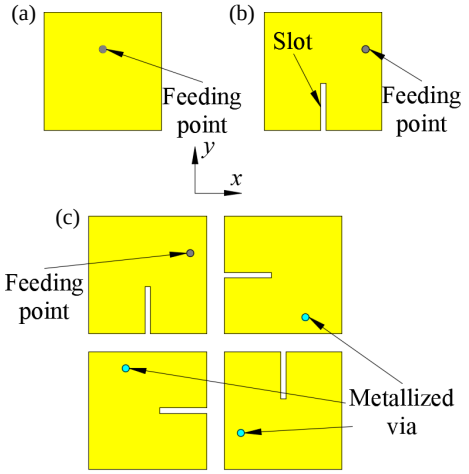

FIGURE 2. Evolutionary design process of the antenna. (a) Case 1, (b) Case 2, (c) Case 3.

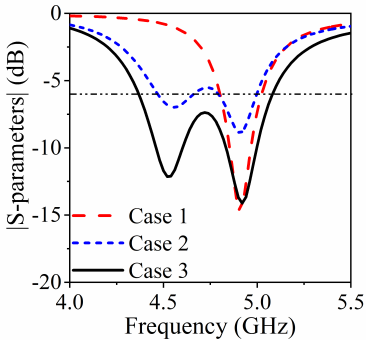

FIGURE 3. The performances of (a) Case 1, (b) Case 2, (c) Case 3.

ing patches also engage, leading to a multi-patch operational mode. It facilitates radiator sharing and significantly enhances the impedance bandwidth compared to a single-patch operation. Subsequently, metallized vias are introduced to adjust and ensure the isolation between elements.

2. ANTENNA CONFIGURATION

The antenna system configuration illustrated in Fig. 1 comprises a MIMO system with four patches. This design includes an antenna substrate (Sub 1), made from FR4 with a dielectric constant of $\varepsilon_{r1} = 4.4$ and a loss tangent of $\tan\delta = 0.02$. The MIMO system consists of four patches, four pairs of metallized vias (Via1), and four feeding vias (Via2). The patches are printed on the upper surface of Sub 1, while Via1 and Via2 are integrated within Sub 1. Each patch corresponds to one slot, with slots etched into the patches to shift TM_{10} mode. Additionally, a metal ground (Ground) is printed on the bottom surface of Sub1. Between each pair of patches, a pair of metallized vias (Via1) is used to adjust the isolation between elements. Each patch is associated with a feed port. Power travels through the metallic vias (Via2) in Sub 1 and is then transferred to the respective patch.

3. ANTENNA DESIGN

3.1. Element Design

First of all, it is worth noting that a current flowing in the x-direction over half a wavelength is defined as TM_{10}, and a current flowing in the y-direction over half a wavelength is defined as TM_{01}. Fig. 2 depicts the evolutionary design process of the antenna, with the performance of each model (Case 1, Case 2, and Case 3) shown in Fig. 3. The initial single element in Fig. 3(a) operates in only one mode, TM_{01}. However, its impedance bandwidth is relatively narrow, covering just 4.5% within the frequency range of 4.8 to 5.02 GHz. To improve the bandwidth, the feed point is shifted to excite TM_{10} mode, as illustrated in Fig. 2(b). A slot was etched into the patch to extend the current paths of TM_{10} without affecting the TM_{01} mode. The slot shifts TM_{10} mode, enabling it to combine with TM_{01} and support dual-mode operation, which covers a bandwidth of 4.47 to 5.0 GHz. To explore the two operating modes, Figs. 4(a) and (b) illustrate the simulated current distributions of Case 2 at two frequencies. At 4.5 GHz, the current flows along the x-

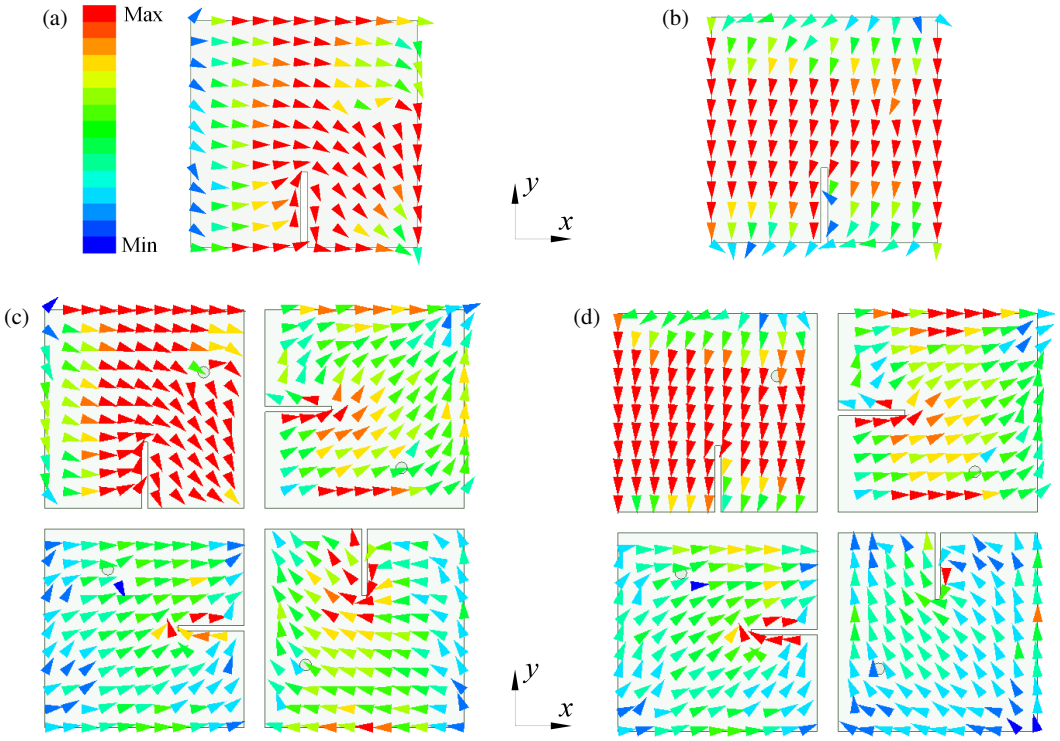

FIGURE 4. Simulated current distribution. (a) Case 2 at 4.5 GHz, (b) Case 2 at 4.9 GHz, (c) Case 3 at 4.5 GHz, (d) Case 3 at 4.9 GHz.

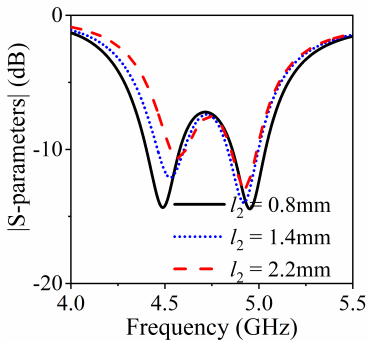

FIGURE 5. The influence of the spacing between patches (l_2) on S-parameter.

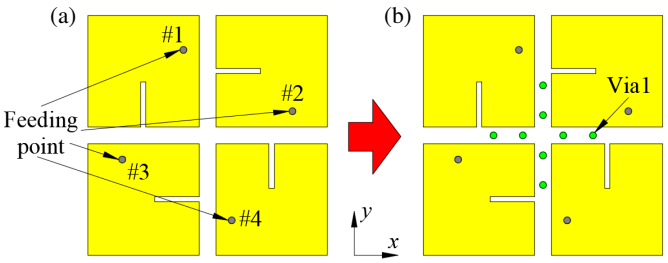

FIGURE 6. Decoupling design of the MIMO system. (a) Case 4, (b) Case 5.

axis, indicating TM_{10} mode. At 4.9 GHz, the current also flows along the y-axis, indicating the TM_{01} mode.

To further enhance the impedance bandwidth, the single patch was converted into a 2×2 multi-patch configuration, as shown in Fig. 2(c). The metallized vias are used to simulate the feeding vias that will be required in the subsequent four-element design. As can be seen from Fig. 3, this modification significantly improved the impedance bandwidth, achieving an enhanced range of 15.3% from 4.36 to 5.08 GHz. To explore the two operating modes, Figs. 4(c) and (d) illustrate the simulated current distributions of Case 3 at two frequencies.

At 4.5 GHz, the patches connected to the feed point operate in TM_{10} mode, with adjacent patches coupled to produce a 45-degree current flow. Similarly, at 4.9 GHz, the patches connected to the feed point operate in the TM_{01} mode, with adjacent patches coupled to produce a 45-degree current flow. This observation confirms that the multi-patch configuration operates effectively. Additionally, a parametric study is performed to analyze the effects of multi-patch configurations. Fig. 5 depicts how patch spacing (l_2) affects $|S_{11}|$. As l_2 decreases, gradual improvement of impedance matching. However, in order to ensure the subsequent isolation, l_2 cannot be too small; therefore, a suitable value was selected.

3.2. MIMO Design

Designed for the four-element MIMO antenna, four ports are introduced, and each is connected to one of the four patches, as shown in Fig. 6. Given the symmetry, port 1 is excited, and element 1 serves as an example. As shown in Fig. 7(a), the isolation between Port 1 and Port 2 exceeds 18 dB because their operational modes have orthogonal polarizations, which results in higher isolation. In contrast, the isolation between Port 1 and Port 3 is over 10 dB due to parallel polarizations of their operational modes, leading to lower isolation.

To achieve good isolation levels across all ports, metallized vias are used to adjust the isolation due to electric field distur-

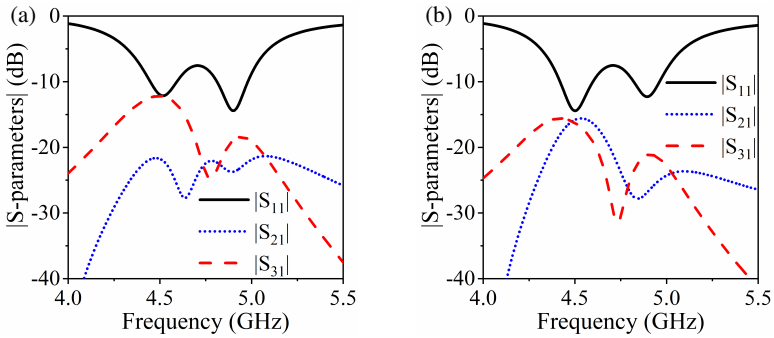

FIGURE 7. Simulated S-parameters of the MIMO system. (a) Without Via1, (b) with Via1.

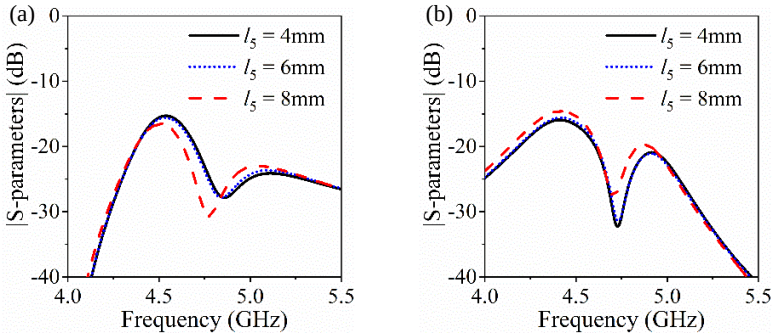

FIGURE 8. The influence of the spacing between patches (l_5) on (a) $|S_{21}|$, (b) $|S_{31}|$.

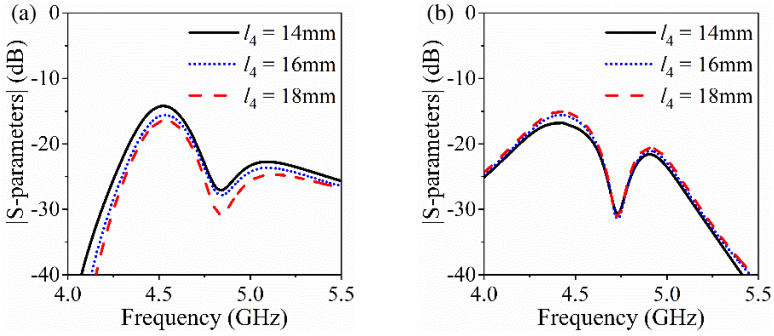

FIGURE 9. The influence of the spacing between patches (l_4) on (a) $|S_{21}|$, (b) $|S_{31}|$.

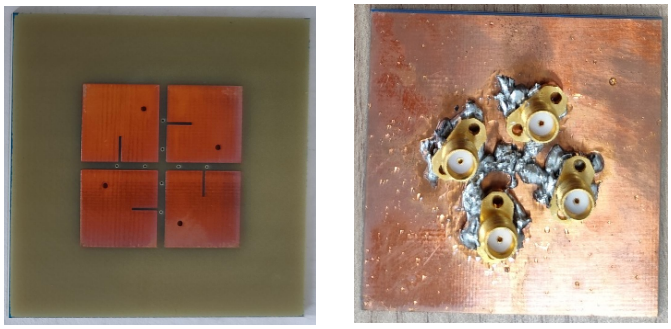

FIGURE 10. Photograph of the antenna prototype: Top view and back view with SMA connectors.

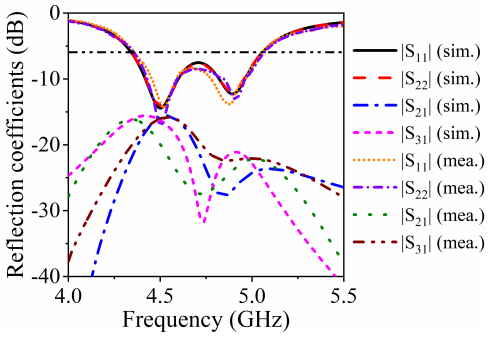

FIGURE 11. S-parameters of the proposed MIMO system.

bances. In case 5 of Fig. 6(b), four pairs of metallized vias were added. As illustrated in Fig. 7(b), the isolation between Port 1 and Port 2, as well as between Port 1 and Port 3, exceeds 15 dB. Given this symmetry, it can be concluded that the isolation between all ports is at least 15 dB. The decoupling mechanism of via1 is illustrated in Fig. 8 and Fig. 9. As l_5 and l_4 increase, the via1 moves outward. $|S_{21}|$ decreases, indicating that the isolation between element 1 and element 2 has been increased; conversely, $|S_{31}|$ increases, meaning the isolation between element

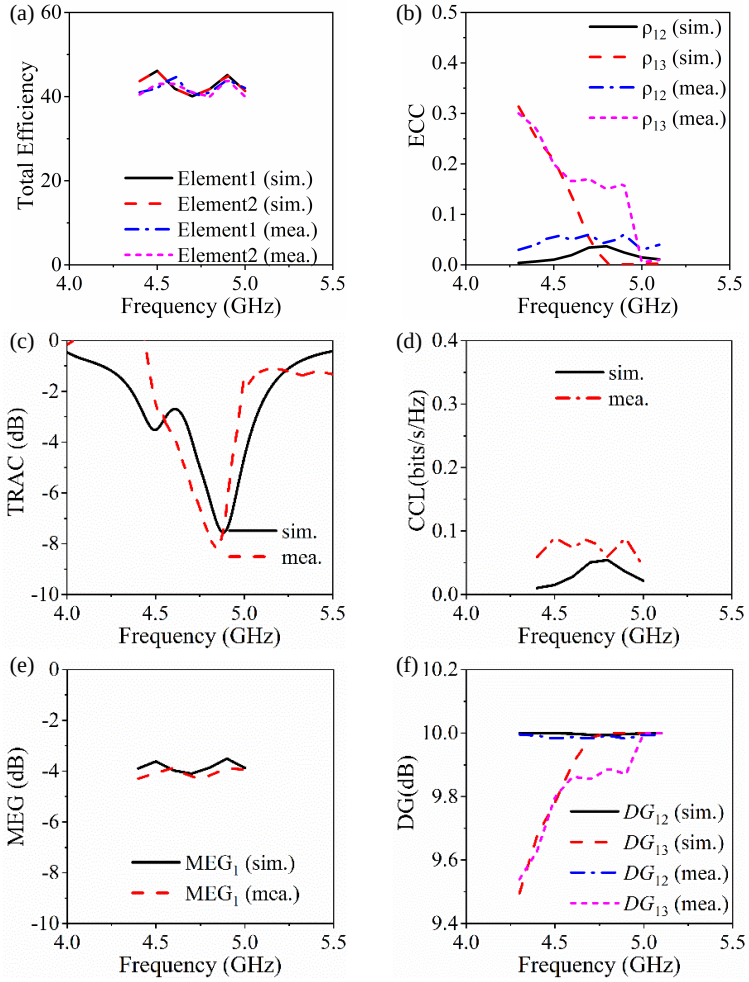

FIGURE 12. Performance of the proposed MIMO system. (a) Total efficiency, (b) ECC, (c) TARC, (d) CCL, (e) MEG, (f) DG.

1 and element 3 has been decreased. Therefore, we selected an appropriate size to ensure that all isolations are above 15 dB.

4. EXPERIMENTAL VERIFICATION

4.1. Measurement Results

To verify the proposed antenna, a prototype has been fabricated and tested. The prototype is depicted in Fig. 10. Each of the four patches is individually connected to one feeding probe.

Figure 11 illustrates the simulated and measured reflection coefficients. The measured −10 dB impedance bandwidth is 15.1% (4.35 GHz to 5.06 GHz), slightly narrower than the simulated bandwidth of 15.3% (4.34 GHz to 5.06 GHz). The mutual coupling between the ports demonstrates good agreement and remains below −15 dB within the impedance bandwidth. Fig. 12(a) presents the simulated and measured total efficiencies within the operational band, exhibits strong agreement. The element achieves total efficiency over 40% in the operational band. The simulated and measured envelope correlation coefficients (ECCs) are depicted in Fig. 12(b). The measured ECC for the antenna is below 0.3, significantly below the threshold of 0.5 [20], indicating favorable performance. The diversity gain (DG), mean effective gain (MEG), channel capacity loss (CCL), and total active reflection coefficient (TARC)

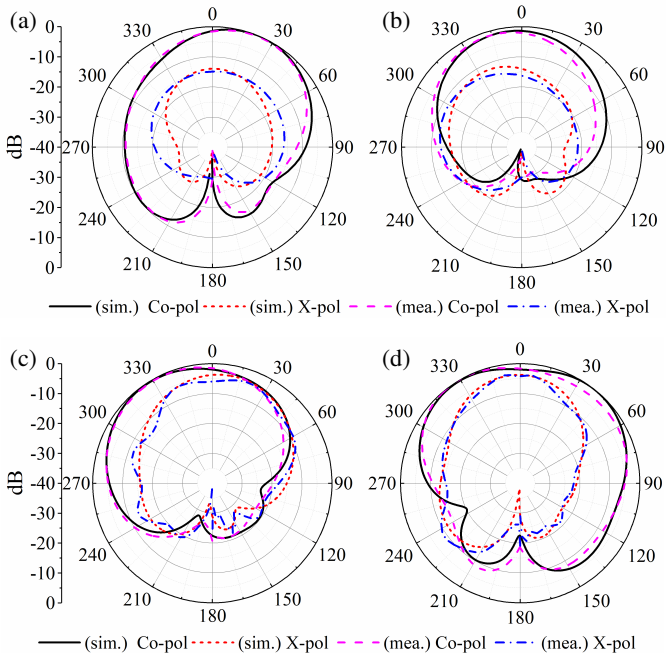

FIGURE 13. Simulated and measured radiation patterns of element 1. (a) 4.5 GHz at xoz-plane, (b) yoz-plane, (c) 4.9 GHz at xoz-plane, (d) yoz-plane.

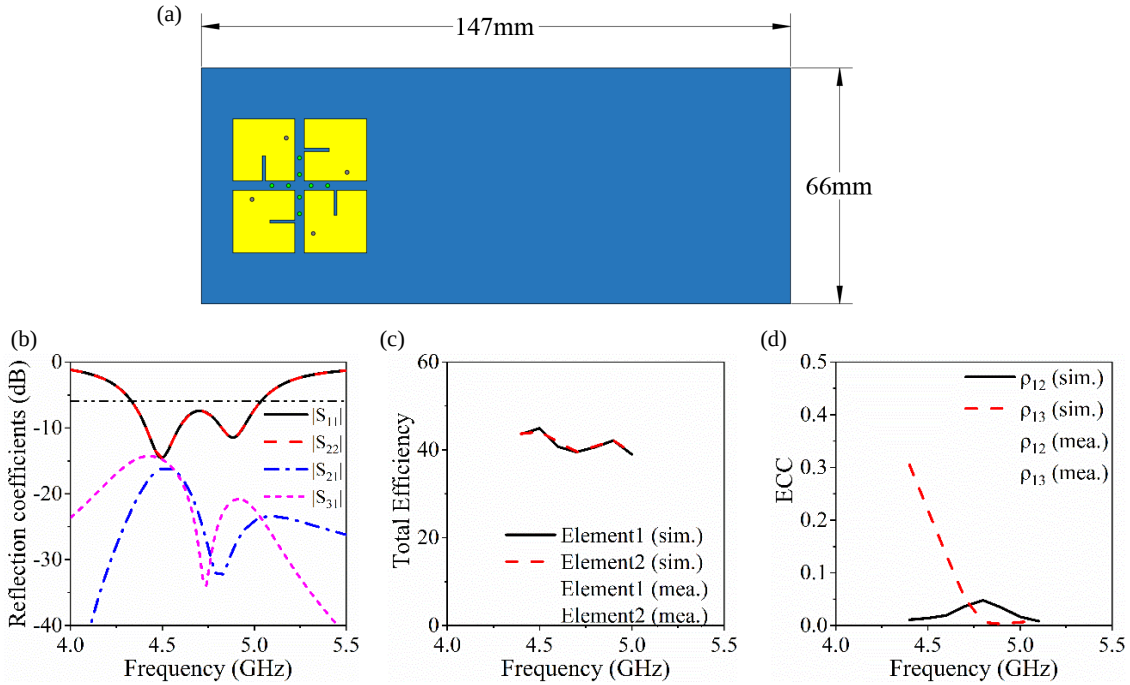

FIGURE 14. (a) Antenna on the phone frame. (b) S-parameters. (c) Total efficiency. (d) ECC.

TABLE 1. Performance comparison with the previous antenna designs.

Ref.	Bandwidth (GHz)	FBW (%)	Efficiency	Isolation (dB)	Electrical Dimension (λ_0^3)	Element Number	Integrate with the Chassis Ground
[15]	3.3–5	41	$>40\%$	>10	$0.581 \times 0.581 \times 0.28$	4	Yes
[16]	3.3–5	41	$>55\%$	>10	$0.82 \times 0.82 \times 0.35$	4	Yes
[17]	3.28–3.85	15.9	$>52\%$	>24	$0.3 \times 0.3 \times 0.02$	2	No
[18]	5.13–5.86	13.3	$>51\%$	>12	$0.27 \times 0.27 \times 0.046$	2	Yes
[19]	4.25–5.13	18.7	$>40.3\%$	>12.5	$0.47 \times 0.47 \times 0.031$	4	Yes
This work	**4.35–5.06**	**15.3**	$>$ **40%**	$>$ **15**	**0.43 × 0.43 × 0.023**	**4**	**Yes**

are shown in Figs. 12(c)–(f). The MIMO antenna system features a TARC below -2 dB, and CCL below 0.1 bits/s/Hz. Due to the structural symmetry, all the four elements should exhibit the same MEG and DG. The element achieves a MEG lying around -4 dB and a DG ranging from 9.6 dB to 10.1 dB. Fig. 13 displays the simulated and measured radiation patterns at 4.5 GHz and 4.9 GHz for Element 1 on the *xoz* and *yoz* planes, showing good agreement. Due to symmetry, it can be inferred that the radiation patterns of each element are complementary, suggesting strong diversity performance and confirming the MIMO system's comprehensive spatial coverage capability.

4.2. Discussion

As shown in Fig. 14, we provide the following parameters of the antenna on the phone frame: S-parameters, total efficiency, and ECC. It can be seen that its performance is almost consistent with the performance of the individually simulated antenna.

Table 1 compares the proposed MIMO antenna with other MIMO antennas. Designs referenced in [15, 16] achieve wideband performance, but they have large sizes and low isolation. In contrast, [17] achieves high isolation over 24 dB with a low profile; however, it is limited to two elements, has a larger planar size, and cannot be directly integrated with the chassis ground. Refs. [18, 19] use shared structure technology to save space, but the designs remain in high profile for compact mobile terminals. This new design offers an effective MIMO solution by maintaining a compact size while ensuring a 15 dB isolation level, making it highly suitable for 5G applications.

5. CONCLUSION

This paper outlines the design, analysis, and experimentation of a compact MIMO antenna system, utilizing shared-radiator technology. By employing a multi-patch operation mode, where excited and neighboring patches jointly radiate, the design achieves a shared-radiator structure that significantly enhances the impedance matching. The addition of metallized vias further ensures isolation between antenna elements. The proposed MIMO antenna not only provides wideband cover-

age, fully encompassing the 5G N79 band, but also maintains a highly compact footprint, making it ideal for modern 5G mobile terminal applications.

REFERENCES

[1] Padhi, J., G. S. Reddy, and C.-Y.-D. Sim, "A surface-mountable electrically small antenna for sub-6 GHz 5G (NR) bands for handheld devices," *IEEE Antennas and Wireless Propagation Letters*, Vol. 24, No. 6, 1402–1406, 2025.

[2] Li, M. and S. Cheung, "Isolation enhancement for MIMO dielectric resonator antennas using dielectric superstrate," *IEEE Transactions on Antennas and Propagation*, Vol. 69, No. 7, 4154–4159, 2021.

[3] Armghan, A., K. Aliqab, V. Sorathiya, F. Alenezi, M. Alsharari, and F. Ali, "Design and fabrication of the split ring resonator shaped two-element MIMO antenna with multiple-band operation for WiMAX/5G/Zigbee/Wi-Fi applications," *Micromachines*, Vol. 13, No. 12, 2161, 2022.

[4] Sun, L., Y. Li, Z. Zhang, and Z. Feng, "Wideband 5G MIMO antenna with integrated orthogonal-mode dual-antenna pairs for metal-rimmed smartphones," *IEEE Transactions on Antennas and Propagation*, Vol. 68, No. 4, 2494–2503, 2020.

[5] Qu, L., H. Kim, K.-Y. Jung, and Y. Liu, "Compact four-port MIMO antenna module with decoupling components for 5G terminal devices," *IEEE Antennas and Wireless Propagation Letters*, Vol. 23, No. 7, 2224–2228, 2024.

[6] Sun, L., Y. Li, and Z. Zhang, "Wideband decoupling of integrated slot antenna pairs for 5G smartphones," *IEEE Transactions on Antennas and Propagation*, Vol. 69, No. 4, 2386–2391, 2021.

[7] Sun, L., Y. Li, and Z. Zhang, "Wideband integrated quad-element MIMO antennas based on complementary antenna pairs for 5G smartphones," *IEEE Transactions on Antennas and Propagation*, Vol. 69, No. 8, 4466–4474, 2021.

[8] Sun, L., Y. Li, Z. Zhang, and H. Wang, "Self-decoupled MIMO antenna pair with shared radiator for 5G smartphones," *IEEE Transactions on Antennas and Propagation*, Vol. 68, No. 5, 3423–3432, 2020.

[9] Yang, B., Y. Xu, J. Tong, Y. Zhang, Y. Feng, and Y. Hu, "Tri-port antenna with shared radiator and self-decoupling characteristic for 5G smartphone application," *IEEE Transactions on Antennas and Propagation*, Vol. 70, No. 6, 4836–4841, 2022.

[10] Cheng, B. and Z. Du, "A wideband low-profile microstrip MIMO antenna for 5G mobile phones," *IEEE Transactions on Antennas and Propagation*, Vol. 70, No. 2, 1476–1481, 2022.

[11] Chang, L. and H. Liu, "Low-profile and miniaturized dual-band microstrip patch antenna for 5G mobile terminals," *IEEE Transactions on Antennas and Propagation*, Vol. 70, No. 3, 2328–2333, 2022.

[12] Chang, L., G. Zhang, and H. Wang, "Triple-band microstrip patch antenna and its four-antenna module based on half-mode patch for 5G 4 × 4 MIMO operation," *IEEE Transactions on Antennas and Propagation*, Vol. 70, No. 1, 67–74, 2022.

[13] Li, K., Y. Zhang, and Y. Li, "Hepta-mode terminal microstrip antenna for mobile Wi-Fi 6/6E and UWB channels 5-11 MIMO applications," *IEEE Transactions on Antennas and Propagation*, Vol. 72, No. 9, 7048–7056, 2024.

[14] Chang, L. and H. Wang, "Miniaturized wideband four-antenna module based on dual-mode PIFA for 5G 4 × 4 MIMO applications," *IEEE Transactions on Antennas and Propagation*, Vol. 69, No. 9, 5297–5304, 2021.

[15] Cheng, S.-H., S.-C. Chen, and W.-Y. Huang, "Low-profile MIMO trapezoidal patch antenna for 5G wideband mobile antenna application," *IEEE Antennas and Wireless Propagation Letters*, Vol. 24, No. 3, 696–700, 2025.

[16] Hu, M. and Y. Li, "Wideband back cover microstrip antenna with multiple shorting vias for mobile 5G MIMO applications," *IEEE Transactions on Antennas and Propagation*, Vol. 71, No. 10, 8290–8295, 2023.

[17] Hu, W., Z. Chen, L. Qian, L. Wen, Q. Luo, R. Xu, W. Jiang, and S. Gao, "Wideband back-cover antenna design using dual characteristic modes with high isolation for 5G MIMO smartphone," *IEEE Transactions on Antennas and Propagation*, Vol. 70, No. 7, 5254–5265, 2022.

[18] Tian, X., J. Wang, C. Zheng, and Z. Du, "Shared-radiator wideband grounded patch antenna pair with bending slot for mobile terminals," *IEEE Transactions on Antennas and Propagation*, Vol. 72, No. 4, 3724–3729, 2024.

[19] Tian, X. and Z. Du, "Wideband shared-radiator four-element MIMO antenna module for 5G mobile terminals," *IEEE Transactions on Antennas and Propagation*, Vol. 71, No. 6, 4799–4811, 2023.

[20] Blanch, S., J. Romeu, and I. Corbella, "Exact representation of antenna system diversity performance from input parameter description," *Electronics Letters*, Vol. 39, No. 9, 705–707, 2003.